Chapter V

Effect of Gamma rays and 90 MeV C^{6+} Ion Beam Irradiation on Optical and Electrical Properties of SiO_2 Doped PVA Nanocomposite Polymer Electrolytes

PVA based nanocomposite polymer electrolyte system with different concentrations of SiO_2 was prepared using the solution casting method. These samples were irradiated with gamma rays and 90 MeV Carbon ion beam. The change in structural, optical and electrical properties due to these irradiations has been studied.

5.1 Introduction

With growing requirements of energy storage and energy conversion devices in daily life, fossil fuel usage has been in demand for the reduction of natural resources and global warming. It is essential to control ongoing imminent hazardous practices of material/process handling. Therefore, the use of biodegradable, less polluting and non-toxic polymer has become more attractive, such as solid polymer electrolytes (SPE) [1]. Recently, many biodegradable polymers have been put to use as solid polymer electrolytes such as polyvinyl alcohol (PVA), polyethylene oxide (PEO), methylcellulose, etc. [2–4]. SPE has potential applications in batteries, fuel cells, supercapacitors, electrochromic display devices and so on [1–3,5–7]. Polyvinyl alcohol (a polar polymer) contains a carbon backbone connecting the hydroxyl group, which has unique properties such as good film-making ability, wide temperature window, biodegradability, nontoxicity and filler-dependent optical and electric properties [8–14]. Many efforts have been made to produce polymer electrolytes which are good proton conductors in anhydrous conditions. H_3PO_4 has been used in the present study, which itself is a good proton conductor due to low acid dissociation constant and extensive self-ionization [15–17]. The chemical stability of PVA could also improve with the addition of solid H_3PO_4.

In contrast to SPE, nanocomposite polymer electrolytes have shown improvement in mechanical strength and ionic conductivity due to the incorporation of ceramic nanofiller such as Al_2O_3, SiO_2, TiO_2, etc., which recently prompted the development of many solid-state device applications [18–21].

Ion beam irradiation is a prominent method to modify the physicochemical properties of polymers. Besides, there is a wide variety of ion species that extend the range of modified polymer applications. These properties designate the ion beam as an excellent and useful tool in improving the optical and electrical properties of polymers. Energetic ions interact with the polymer by producing reactive radicals that, in turn, create cross-links and new functional groups [1–3]. For ion beam irradiation, the target is ionized directly to prompt cleavage, degradation, emission of atoms and gases. Energetic ions non-uniformly lose their energy to produce cylindrical zones, while the gamma rays uniformly modify the polymer's entire volume [22,23].

The present work's objective is to develop PVA-H_3PO_4 polymer electrolytes with different SiO_2 nanoparticle dopant concentrations and study the effect of gamma and carbon ion irradiation on their structural, optical and ion transport properties. These properties of pristine and irradiated PVA/H_3PO_4/SiO_2 nanocomposite polymer electrolytes (PHS) have been studied using XRD, UV-Visible and impedance spectroscopies [24,25].

5.2 Results and Discussion

5.2.1 XRD analysis

Figures 5.1 & 5.2 present X-ray diffraction patterns of pristine and irradiated PVA/H_3PO_4/SiO_2 nanocomposite polymer electrolytes. The XRD measurement was carried out in the 2Θ range from 10º to 60º, to correlate the variation in structure, if any, with the concentration of SiO_2 and irradiation dose. The XRD diffraction pattern of PVA was observed to manifest characteristic peaks around 2Θ = 19.6º and 41º. The intense peak in the diffraction pattern of PVA indicates that the polymer is semicrystalline. It also describes strong inter and intramolecular hydrogen bonding in each monomer unit in PVA [26]. There is no peak observed other than that of PVA, implying complete dissociation of the acid.

As the concentration of nanofiller increases, the intensity of the major peak of PVA decreases with broadening. It suggests an increase in the amorphous phase, with an increase in the concentration of nanoparticles. The nanoparticles can cause significant disorders, resulting in a decrease in crystallinity. Further, after gamma rays and SHI irradiations, there is a decrease in the peak intensity of PHS10 nanocomposite polymer electrolyte along with broadening. These results could be due to the rupture of several bonds and release of volatile gases - possible phenomena responsible for developing more disordered systems [27]**.** Both kinds of radiation cause excitation or ionization of atoms and molecules of the polymer. They also cause the migration of atoms from their original sites to neighbouring lattice sites [28]. After both types of irradiations, a decrease in crystallinity is indicated by the fall in peak intensity with broadening.

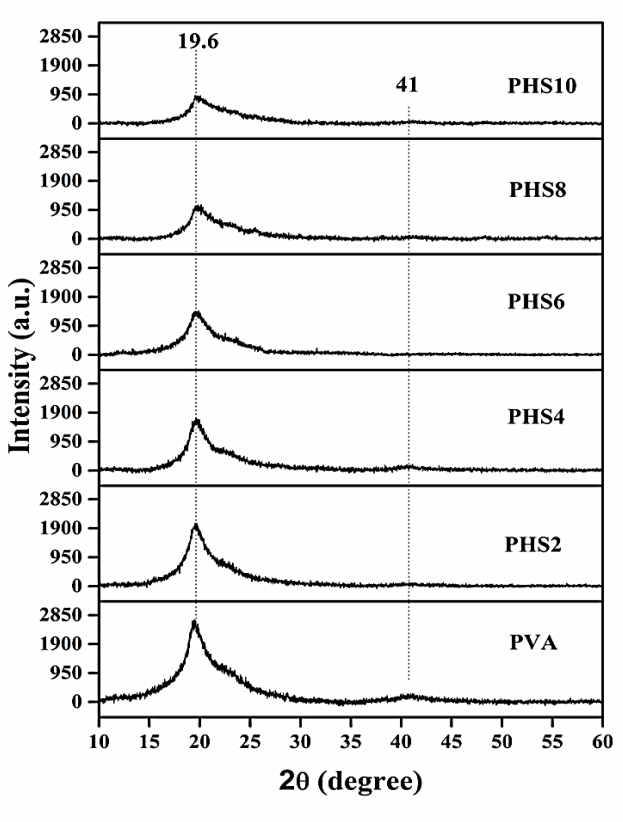

Figure 5.1 XRD plots of PVA and pristine PHS nanocomposite polymer electrolytes.

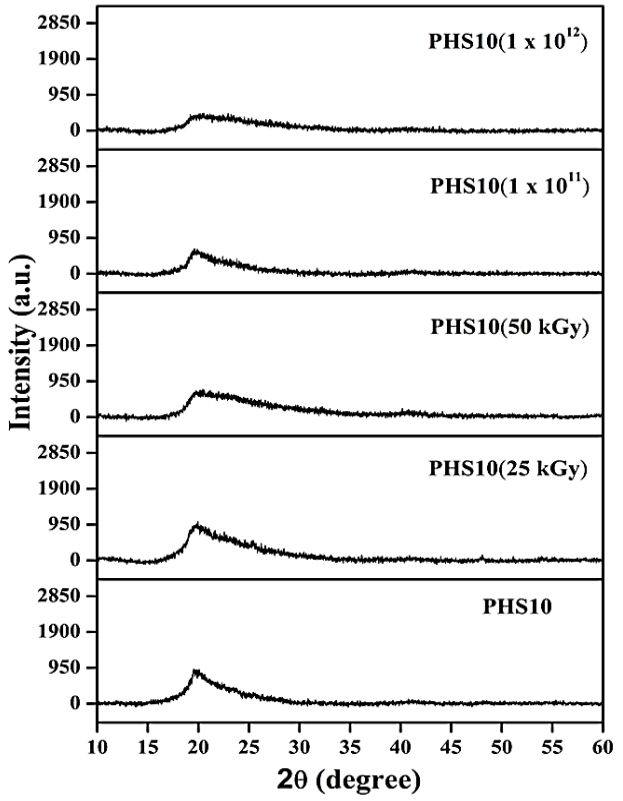

Figure 5.2 XRD plots of irradiated PHS10 nanocomposite polymer electrolytes.

5.2.2 Fourier Transform Infrared Spectroscopy

Fourier transform infrared spectroscopy is employed to study intermolecular interaction and complex formation of nanocomposite polymer electrolytes. Figure 5.3 shows FTIR spectra of pure PVA. In FTIR spectra of PVA, the broad absorption peak in the range of 3000-3600 cm^{-1} represents O-H symmetric stretching vibration. It arises from inter and intramolecular hydrogen bonds in the polymer matrix. The peaks at 1092 cm^{-1} and 852 cm^{-1} are attributed to hydroxyl C-O stretching and CH_2 stretching vibrations, respectively. The vibrational bands at 1411, 1650 and 2957 cm^{-1} can be ascribed to CH_2 bending vibrations, acetyl C=C stretching and CH_2 asymmetric stretching, respectively. The band at 1258 cm^{-1} describes C–H wagging mode and C–O stretching of acetyl group [29].

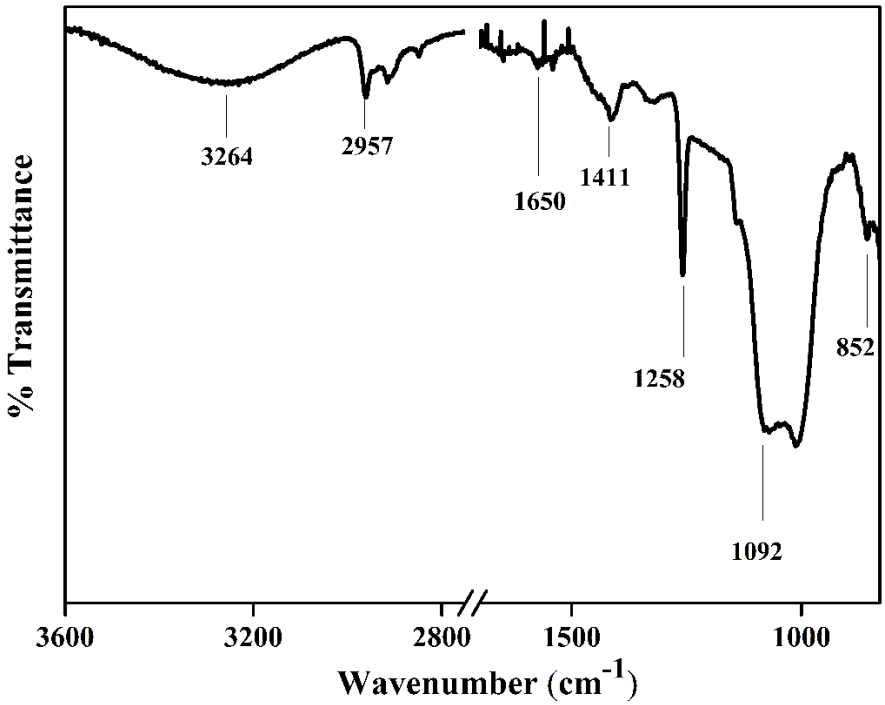

Figure 5.3 FTIR spectrum of pure PVA

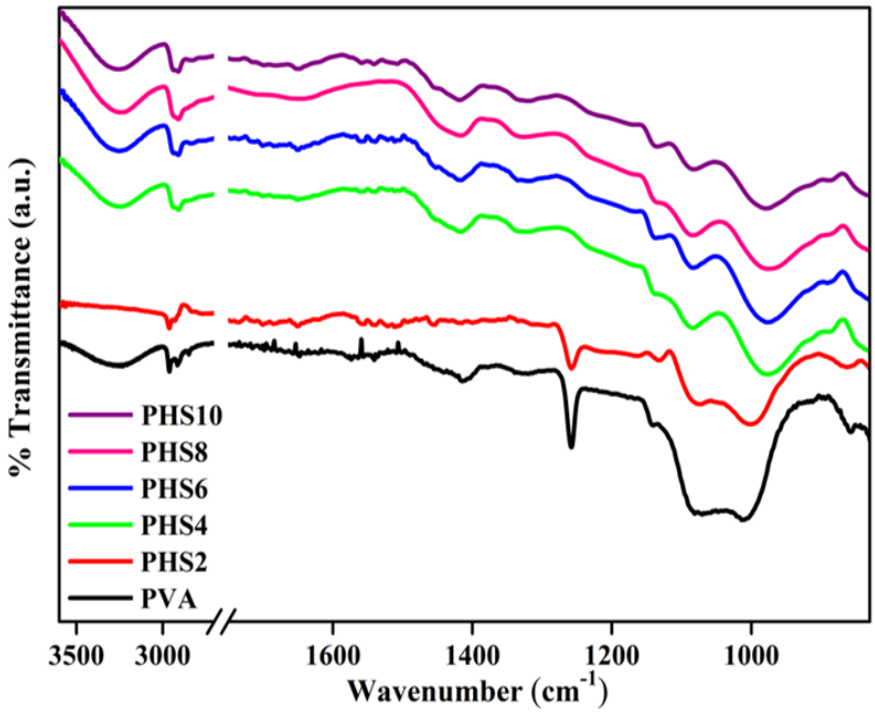

Figure 5.4 FTIR spectra of Pure PVA and PHS nanocomposite polymer electrolytes.

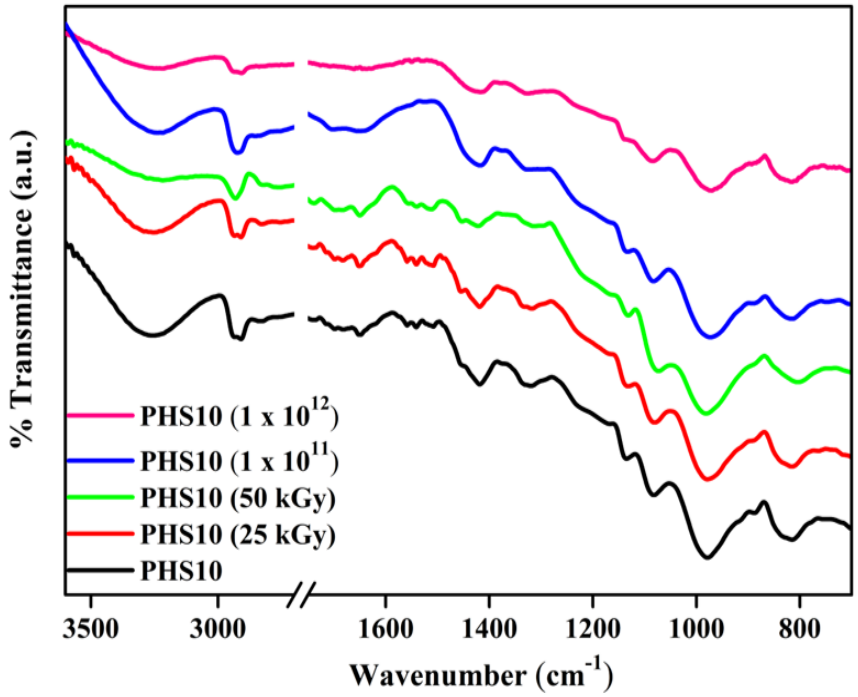

Figure 5.5 FTIR spectra of gamma rays and SHI irradiated PHS10 nanocomposite polymer electrolytes.

Figures 5.4 and 5.5 depict the FTIR spectra of pristine and irradiated nanocomposite polymer electrolytes, respectively. After incorporating nanoparticles, the peaks in the region of 850-1200 cm^{-1} have been found to decrease. The inclusion of SiO_2 in polymer electrolytes increases the free volume. Thus, the sample becomes more amorphous [30]. Also, it indicates the interaction of nanoparticles with the polymer electrolyte. The FTIR spectra of irradiated samples show a decrease in all vibrational bands' intensity with irradiation dose. This result implies a sharp modification of the material by both kinds of irradiations. S_e value of C^{6+} ions is of the order of keV/nm, as calculated from SRIM-2008. This result suggests that swift heavy ions are very efficient in breaking all linkages in a range of a few nanometers along their path. In the gamma irradiation case, the ionization of target atoms occurs through secondary electrons. Therefore, when gamma rays pass through a polymer, only a fraction of the energy is used to modify the material [23,31]. Moreover, after irradiation, a decreased intensity of vibration bands can be attributed to altering the bond structure due to removing hydrogen from the backbone and the side-chain. It also suggests chain scission of the polymeric matrix.

5.2.3 UV-Visible Analysis

Variation of absorbance with the concentration of SiO_2 nanoparticles and irradiation dose is depicted in figures 5.6 & 5.7. The absorption spectrum of pure PVA is characterized by an absorption band at 275 nm, resulting from $n \rightarrow \pi^*$ transition of C=O group of polymer matrix [32]. The absorption is observed to increase with the concentration of SiO_2 nanoparticles and irradiation dose. This could be due to the creation of a charge-transfer complex that delocalized conduction electrons. The absorption edge of PHS10 after irradiation is seen to shift towards a longer wavelength; this could be owing to a change in the structure via randomization of macromolecular chains and destroying properties of polymeric linkage [1]. This result shows a reduction in the optical bandgap.

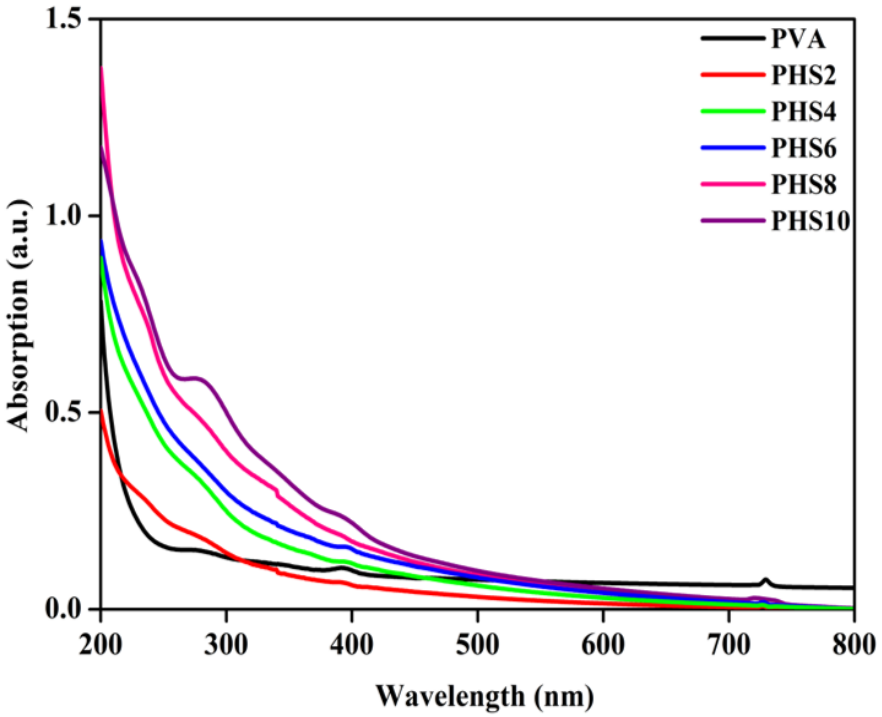

Figure 5.6 Absorption spectra of PVA and pristine PHS nanocomposite polymer electrolytes.

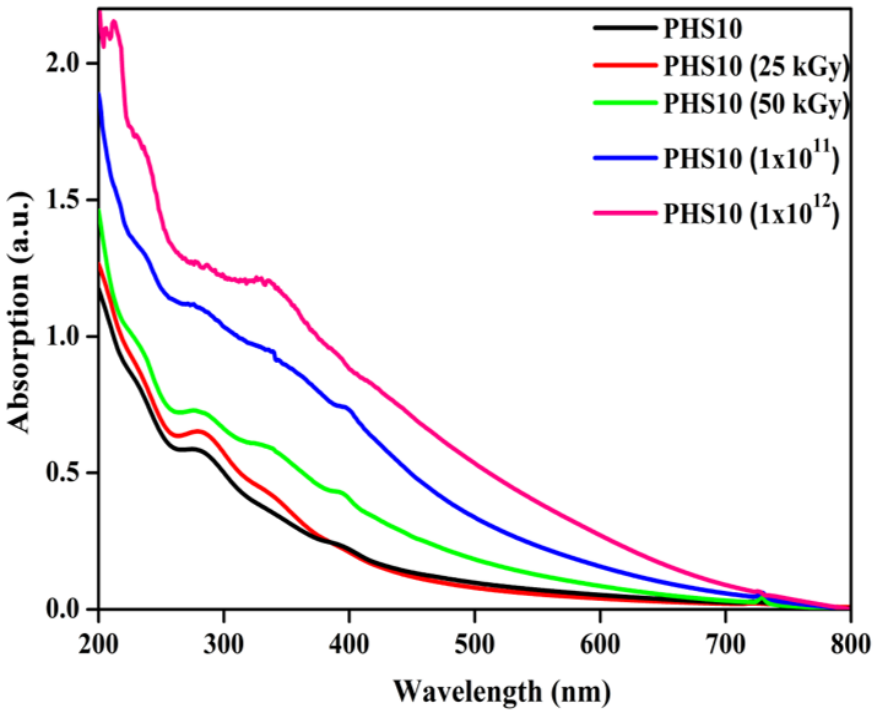

Figure 5.7 Absorption spectra of gamma and SHI irradiated PHS10 nanocomposite polymer electrolytes.

Sample	Bandgap (eV)	Number of carbon atoms (M)
PVA	5.19	43.67
PHS2	4.29	63.92
PHS4	4.15	68.31
PHS6	4.05	71.72
PHS8	3.85	79.37
PHS10	3.78	82.33
PHS10 (25 kGy)	3.73	84.56
PHS10 (50 kGy)	3.54	93.88
PHS10 (1 x 10^{11})	3.35	104.83
PHS10 (1 x 10^{12})	3.23	112.76

Table 5.1 Optical band gap of pristine and irradiated PHS.

The modification of indirect optical bandgap (E_g) due to the incorporation of nanoparticles and irradiation was determined using Tauc's relation [33]. It was determined by extrapolating intercept on the X-axis (energy axis) of the plot of $(\alpha hv)^{1/2}$ versus (hv). The observed decreasing values of optical bandgap with the concentration of SiO_2 and irradiation dose are shown in Table 5.1. The reduction in the energy gap due to nanoparticles' addition indicates the interaction of polymer electrolyte with nanoparticles and the formation of localized states between HOMO and LUMO energy bands, which increases the probability of lower transition energy.

Further, the reduction in the optical bandgap of post-irradiated also results from the creation of unsaturated bonds. These results indicate an increase in the number of charge carriers and lower energy required to transition from HOMO to LUMO bands [32]. A decrease in bandgap indicates an increment in conductivity.

Moreover, Swift heavy ions effectively produce structural disorders and more radicals in the host matrix than gamma rays irradiation, which could be described based on the density of state model in amorphous solids, given by Mott and Davis [34].

The number of carbon atoms per conjugation length (M) was determined using the following equation [35]:

$$E_g = \frac{34.3}{\sqrt{M}}\ eV$$

The values of M for pristine and irradiated samples are listed in table 5.1. These are found to increase with increasing irradiation dose due to an increase in the dehydrogenation process [23].

5.2.4 AC Electrical Properties

5.2.4.1 Dielectric Analysis

Frequency-dependent complex dielectric function, ε* is given by ε*(ω) = ε′(ω) - ε"(ω) and related to molecular relaxation as well as transport properties of the system. The real part ε′(ω) of complex permittivity is related to the capacitance, whereas, the imaginary part ε"(ω) is associated with the conductance. The variation in the real part of permittivity of pristine and irradiated PHS are illustrated in figures 5.8 & 5.9, respectively, whereas the imaginary part of permittivity of pristine and of irradiated nanocomposite polymer electrolytes are shown in figures 5.10 & 5.11, respectively. ε′(ω) and ε"(ω) show a tendency to increase with decreasing frequency in the low-frequency range for all the samples, a phenomenon which can be ascribed to the occurrence of space charge/interfacial polarization at the boundary of the polymer electrolyte and the electrode. As frequency increases, ε′(ω) and ε"(ω) are observed to decrease, which may be ascribed to the failure of the induced dipole to rotate with periodic reversal of the field. The contributions of orientational and ionic polarizabilities are reduced with increasing frequency. Then they altogether disappear because of the inertia of mobile ions, which makes the real and imaginary part of dielectric permittivity constant at high frequencies [36]. ε′(ω) and ε"(ω) are seen to increase with an increase in the concentration of SiO_2 nanoparticles, which is related to the interfacial polarization effect between PVA matrix and SiO_2 nanoparticles.

Furthermore, the ε′(ω) and ε"(ω) increase with increasing radiation dose. It could be due to the increase of the polymer chains' mobility as a result of the

breaking of several bonds. Swift heavy ions trigger a significant degradation of the sample and, therefore, increase the dielectric response.

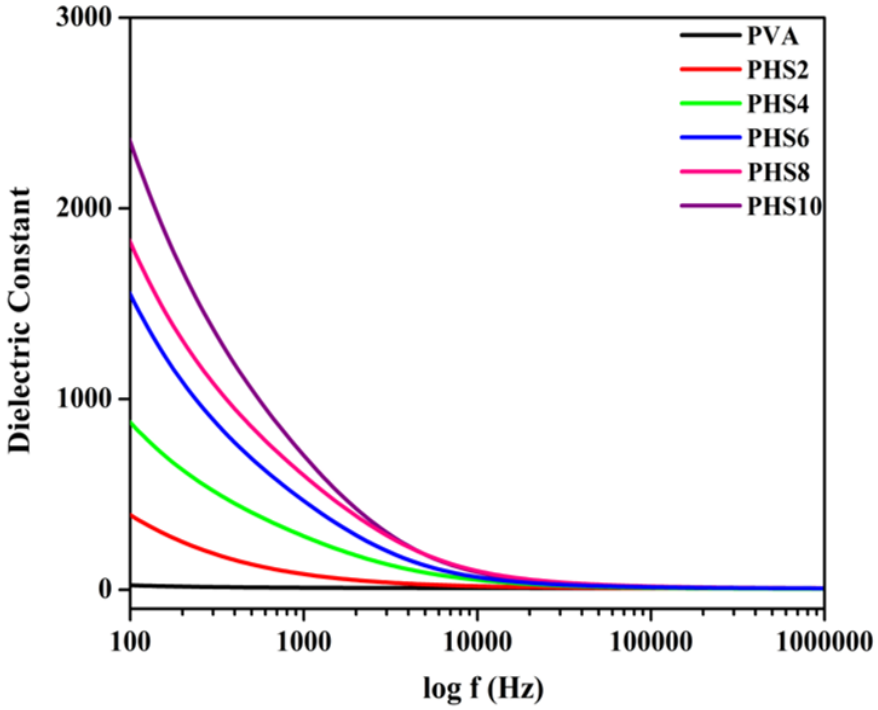

Figure 5.8 Frequency-dependent dielectric constant of PVA and pristine PHS nanocomposite polymer electrolytes.

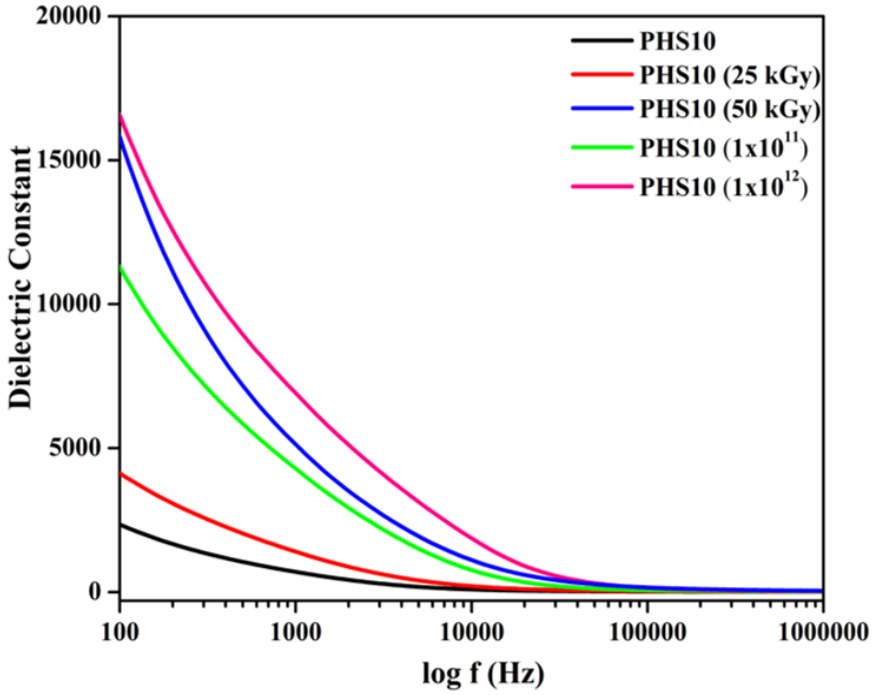

Figure 5.9 Frequency-dependent dielectric constant of irradiated PHS10 nanocomposite polymer electrolytes.

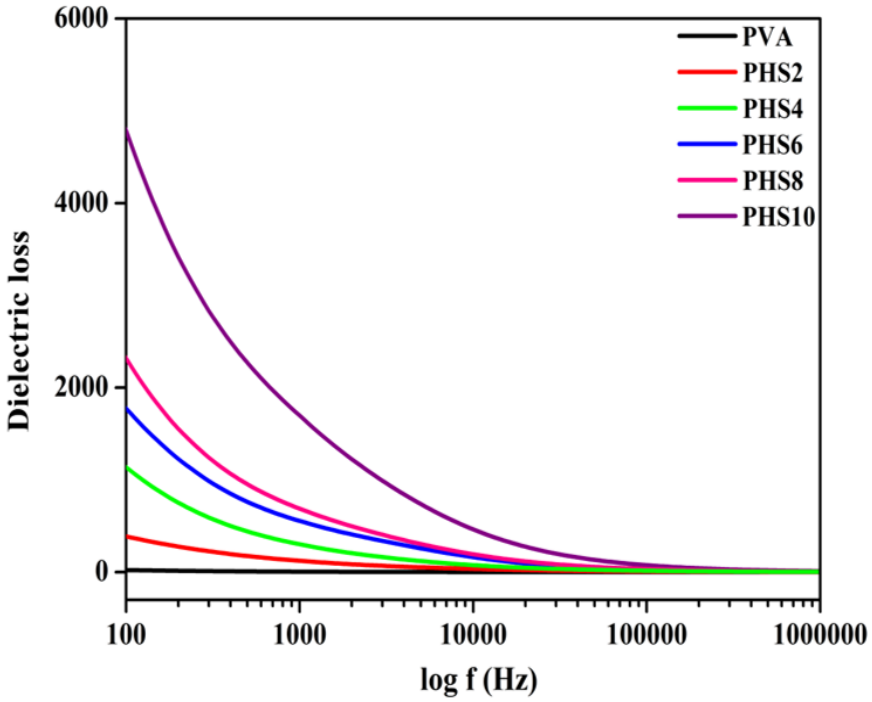

Figure 5.10 Frequency-dependent dielectric loss of PVA and pristine PHS nanocomposite polymer electrolytes.

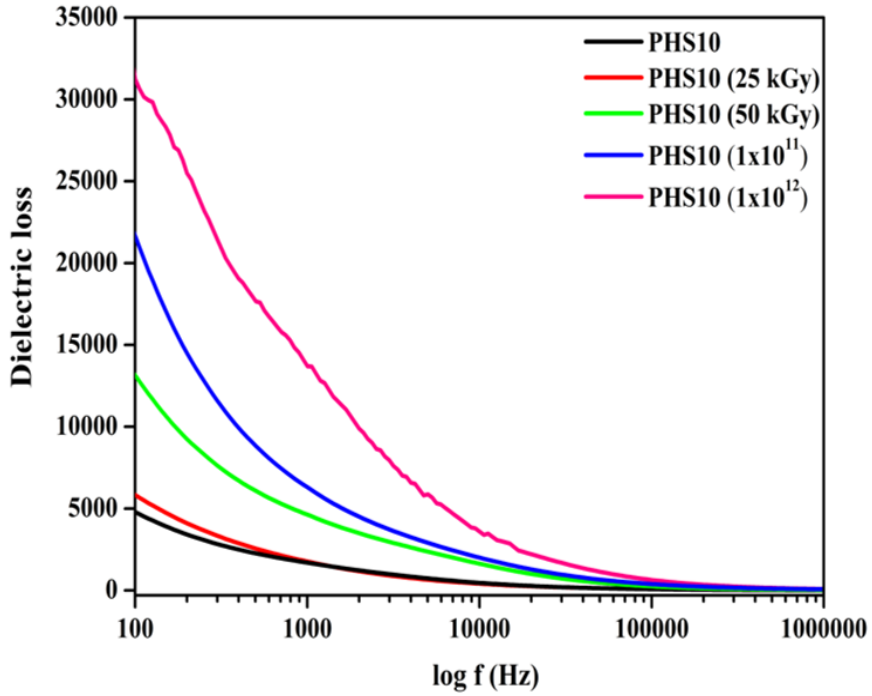

Figure 5.11 Frequency-dependent dielectric loss of irradiated PHS10 nanocomposite polymer electrolytes.

5.2.4.2 Complex Impedance Analysis

Complex impedance spectroscopy is an important technique to study the electrical properties of a solid. It is often employed to determine the bulk conductivity of the system. Impedance plots of PHS for different filler levels of nanoparticles and irradiation doses are shown in figure 5.12. This figure displays a high-frequency depressed semicircle followed by a low-frequency spike. The high-frequency semicircle relates to the relaxation process connected to the bulk region. The low-frequency region is a consequence of the electrode blocking effect and the intercept of the spike on the X-axis gives the value of bulk resistance. Figure 5.12 shows that the value of bulk resistance decreases with increasing concentration of nanoparticles and irradiation dose. This must-have enhanced amorphicity by offering a new conducting path which increases ionic conductivity.

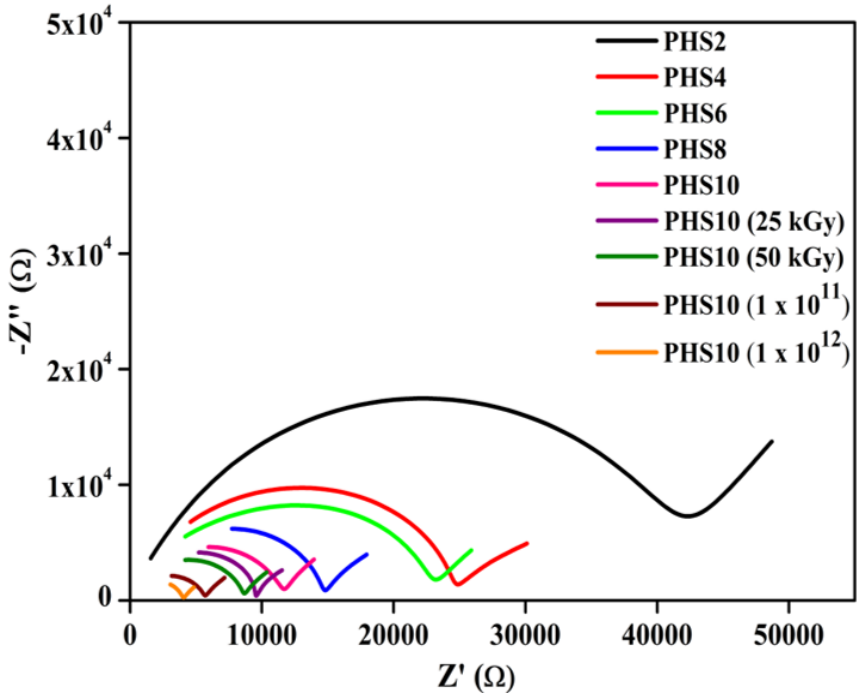

Figure 5.12 Cole-Cole plot of pristine and irradiated PHS nanocomposite polymer electrolytes.

Sample	DC conductivity (S cm^{-1}) (from bulk resistance)
PHS2	0.0000865
PHS4	0.000144
PHS6	0.000153
PHS8	0.000252
PHS10	0.000271
PHS10 (25 kGy)	0.000307
PHS10 (50 kGy)	0.000407
PHS10 (1 x 10^{11})	0.000808
PHS10 (1 x 10^{12})	0.000881

Table 5.2 DC Conductivity for PHS nanocomposite polymer electrolyte.

The ionic conductivity (σ) of PHS is determined from bulk resistance (R_b), the contact area of electrode-electrolyte interface and thickness of the sample using the equation:

$$\sigma = \frac{t}{A R_b}$$

The calculated value of DC conductivity of PHS is shown in Table 5.2. It is observed that the value of the ionic conductivity of PHS increases with increasing concentration of nanoparticles and irradiation dose. This resulted in a decrease in the degree of crystallinity and promoting ionic and segmental mobilities. The ionic conductivity of SHI irradiated PHS10 system is higher than that of the gamma-irradiated system.

5.2.4.3 AC Electrical Conductivity

The frequency-dependent AC conductivity plots for pristine and irradiated nanocomposite polymer electrolytes at constant temperature are shown in figures 5.13 & 5.14. The frequency-dependent AC conductivity plots include three distinct regions: (i) the high-frequency dispersion region, which is the result of short-range ion transport related to the hopping of charge carriers (ii) the intermediate region associated with long-range diffusion of ions and dc conductivity (iii) the low-frequency dispersion region, which can be attributed to the electrode polarization at the electrode-electrolyte interface [37].

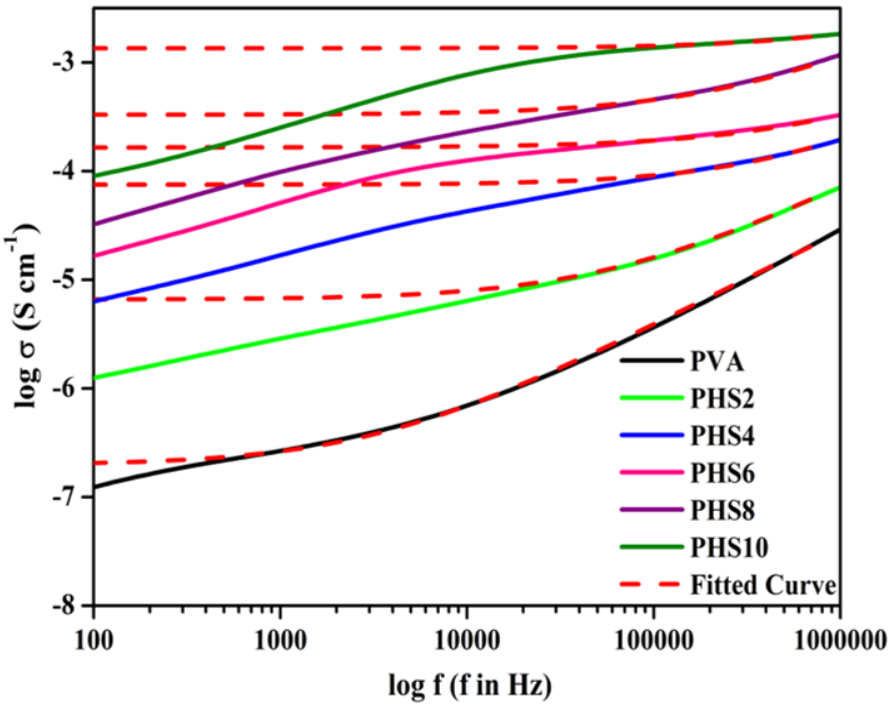

Figure 5.13 Frequency-dependent AC conductivity of PVA and pristine PHS nanocomposite polymer electrolytes.

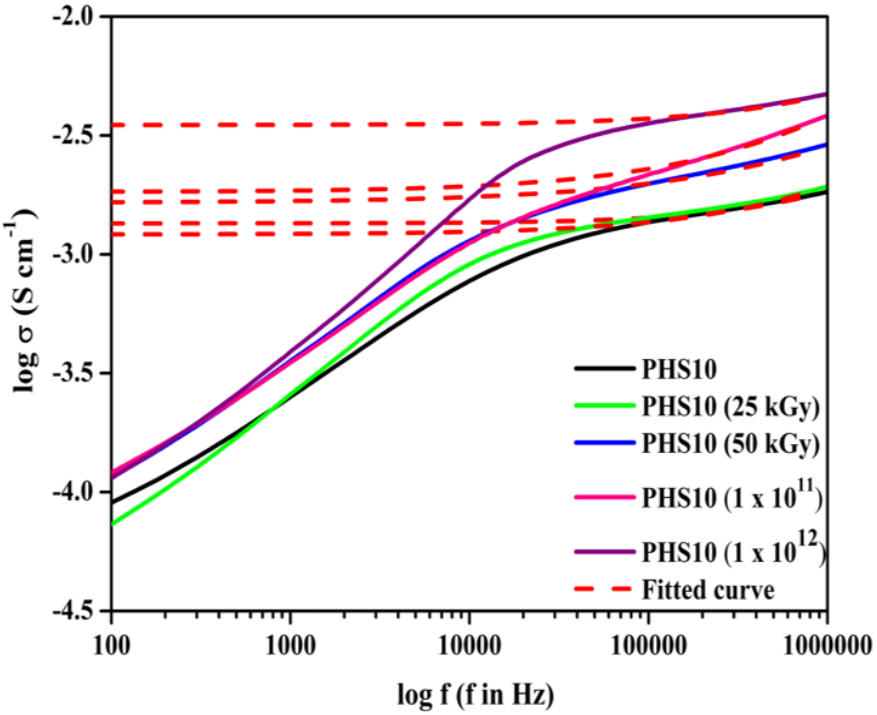

Figure 5.14 Frequency dependent AC conductivity of PVA and irradiated PHS10 nanocomposite polymer electrolytes.

Sample	σ_{dc} (S cm^{-1})	A	Frequency Exponent (n)
PVA	1.968 x 10^{-7}	1.6 x10^{-10}	0.873
PHS2	6.58 x 10^{-6}	6 x 10^{-10}	0.84
PHS4	0.75 x 10^{-4}	6.55 x 10^{-10}	0.78
PHS6	1.0 x 10^{-4}	7.21 x 10^{-10}	0.702
PHS8	1.65 x 10^{-4}	3.0 x 10^{-10}	0.702
PHS10	3.3 x 10^{-4}	9.0 x 10^{-9}	0.682
PHS10 (25 kGy)	1.21 x 10^{-3}	6.9x 10^{-9}	0.678
PHS10 (50 kGy)	1.35 x 10^{-3}	6.83 x 10^{-8}	0.671
PHS10 (1 x 10^{11})	1.65 x 10^{-3}	6.0 x 10^{-8}	0.637
PHS10 (1 x 10^{12})	3.5 x 10^{-3}	5.82 x 10^{-8}	0.619

Table 5.3 Fitting parameters from Jonscher's power law σ_{dc}, A and n for PHS.

The AC conductivity (σ_{ac}) follows the Jonscher universal power law, given as:

$$\sigma_{ac} = \sigma_{dc} + A\,\omega^{n}$$

where, σ_{dc} is DC conductivity, A and n ($0 < n < 1$) are pre-exponential parameter and power-law exponent, respectively [37].

The values of σ_{dc}, A and n for pristine and irradiated PHS are listed in Table 5.3. The value of n varies between 0.619-0.873, suggesting the hopping of charge carrier responsible for conduction. The increasing trend of DC conductivity can be ascribed to the reduction in crystallinity with the increasing mobility of charge carriers. AC conductivity of irradiated nanocomposite polymer electrolyte is higher than that of the pristine PHS. As the gamma irradiation dose and ion fluence increase, there is an increase in the amount of local energy deposition, implying an increase in free electron and impurity concentrations. These could suggest the formation of carbon-rich localized networks and the scission of macromolecular chains [1,23]. The value of LET of carbon ions is greater than that of gamma rays [38]. Thus the effect of gamma irradiation on electrical properties of PHS10 is less than that of swift heavy ion irradiation.

5.2.5 Differential Scanning Calorimetry Analysis

The effect of irradiation on the thermal properties and degree of crystallinity of PHS10 were investigated using DSC thermograms, as depicted in Figure 5.15. DSC thermograms of pristine and irradiated PHS10 show the same trends, i. e., exhibiting endothermic peaks. This endothermic peak corresponds to the melting temperature of PVA in polymer complexes and explains the phase transition from the semicrystalline phase to the amorphous phase. The change in the degree of crystallinity was calculated using the formula [39]:

$$X_c = \frac{\Delta H_m}{\Delta H_{m,0}}$$

where, ΔH_m is the enthalpy of fusion for PVA, while $\Delta H_{m,0}$ is fusion enthalpy for 100% crystalline material and is taken to be 138.6 J/g for PVA [40]. The relative degree of crystallinity ($\Delta X_c\%$) of PHS10 is reduced after gamma and SHI irradiations, as shown in Table 5.4. The melting point of PHS10 is observed to shift towards the lower temperature after irradiation, suggesting a decrease of molecular weight due to scissioning of the polymer chain. It also implies the amorphization of the polymer matrix due to irradiation [41]. The DSC results are consistent with the results obtained from XRD and FTIR analyses.

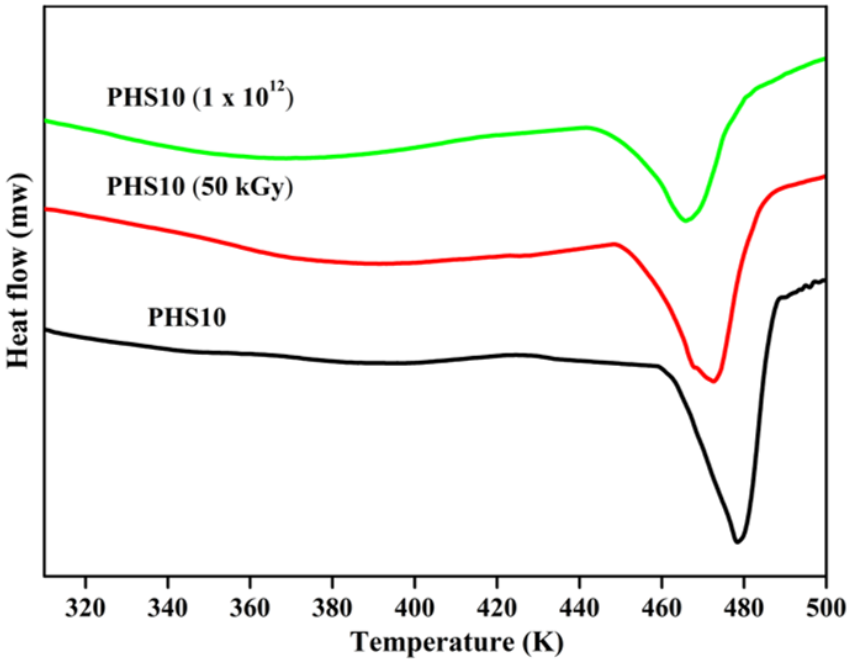

Figure 5.15 DSC thermogram of pristine and irradiated PHS10 nanocomposite polymer electrolytes.

Sample	T_m (K)	X_C%
PHS10	479.08	70.15
PHS10 gamma irradiated (50 kGy)	472.96	67.08
PHS10 SHI irradiated (1×10^{12} ions/cm^2)	465.72	48

Table 5.4 Melting Temperature and degree of crystallinity upon gamma rays and 90 MeV carbon ion irradiations.

5.2.6 Surface Morphology

Three-dimensional scanned topographical image of pristine and irradiated nanocomposite polymer electrolytes was obtained using AFM in tapping mode. The image is shown in figure 5.16. It was analyzed employing average surface roughness (R_a). The average roughness R_a of pristine PHS10 was found to be 92 nm, whereas those of the SHI irradiated PHS10 (1×10^{12}) and gamma-irradiated PHS10 (50kGy) was found to be 82 nm and 86 nm, respectively. Highly excited zones are developed over the surface of the polymer upon SHI irradiation. In the case of gamma irradiation, a small amount of its energy dissipates in material to modify polymeric material, whereas swift heavy ions lose whole energy to modify the material. The roughness changes detected in the case of gamma irradiation are less than those in the case of ion beam irradiation due to the lesser transfer of energy by gamma radiation than by ions [23]**.** Thus the surface of irradiated polymeric material became smoother than the pristine polymeric material.

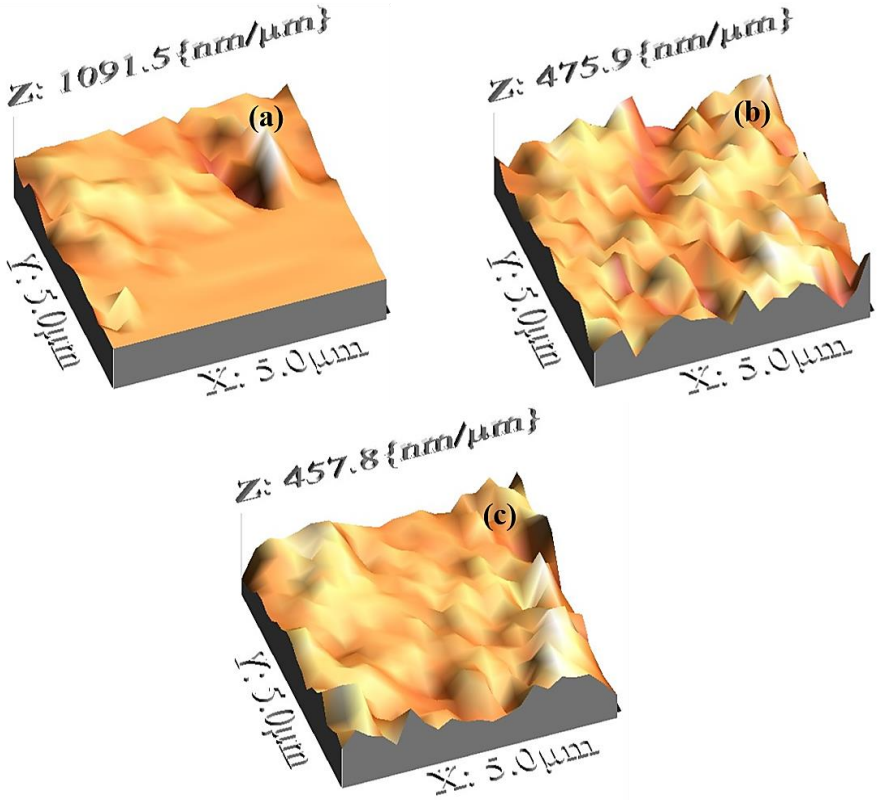

Figure 5.16 AFM image of (a) PHS10, (b) PHS10 (50 kGy) (c) PHS10 (1 x 10^{12}).

5.3 Conclusion

PVA/H_3PO_4/SiO_2 nanocomposite polymer electrolyte was prepared via solution casting method and irradiated with gamma rays and 90 MeV carbon ions. From XRD analysis, the system's crystallinity was found to decrease, which is correlated to the result obtained from DSC. FTIR analysis confirms the occurrence of phenomena such as complexation and interaction due to the incorporation of filler. Alteration of the FTIR peak intensity of functional groups upon gamma and ion beam irradiation is ascribed to the breakage of a few bonds and the creation of free radicals due to gamma and ion beam irradiations. It was observed that the optical bandgap of the system decreases with the concentration of the filler and radiation dose. The increase in dielectric response with radiation dose is a consequence of the change in physicochemical properties. Frequency-dependent AC conductivity follows Jonscher's power law, and the charge conduction in the system can be attributed to the hopping mechanism. AFM study indicates that the system's low value of average surface roughness accounts for easier ionic conduction. For almost all measured parameters, swift heavy ion irradiated nanocomposite polymer electrolytes underwent significant changes compared to those of gamma-irradiated.

References:

[1] G. B. Patel, N. L. Singh, F. Singh, Modification of chitosan-based biodegradable polymer by irradiation with MeV ions for electrolyte applications, Mater. Sci. Eng. B. 225 (2017) 150–159. https://doi.org/10.1016/j.mseb.2017.08.023.

[2] S. Sreepathirao, K. Satyanarayanrao, M. Shareefuddin, U. Subbarao, S. Chandra, Ionic conductivity and battery characteristic studies on PEO+$AgNO_3$ polymer electrolyte, Solid State Ionics. 67 (1994) 331–334. https://doi.org/10.1016/0167-2738(94)90026-4.

[3] S. Liang, J. Yang, X. Zhang, Y. Bai, The thermal-electrical properties of polyvinyl alcohol/$AgNO_3$ films, J. Appl. Polym. Sci. 122 (2011) 813–818. https://doi.org/10.1002/app.34060.

[4] N. E. A. Shuhaimi, N. A. Alias, M. Z. Kufian, S. R. Majid, A. K. Arof, Characteristics of methyl cellulose-NH_4NO_3-PEG electrolyte and application in fuel cells, J. Solid State Electrochem. 14 (2010) 2153–2159. https://doi.org/10.1007/s10008-010-1099-4.

[5] S. B. Aziz, Z. H. Z. Abidin, A. K. Arof, Effect of silver nanoparticles on the DC conductivity in chitosansilver triflate polymer electrolyte, Phys. B Condens. Matter. 405 (2010) 4429–4433. https://doi.org/10.1016/j.physb.2010.08.008.

[6] N. M. Morni, A. K. Arof, Chitosan–lithium triflate electrolyte in secondary lithium cells, J. Power Sources. 77 (1999) 42–48. https://doi.org/10.1016/S0378-7753(98)00170-0.

[7] K. R. Mohan, V. B. S. Achari, V. V. R. N. Rao, A. K. Sharma, Electrical and optical properties of (PEMA / PVC) polymer blend electrolyte doped with $NaClO_4$, 30 (2011) 881–886. https://doi.org/10.1016/j.polymertesting.2011.08.010.

[8] J. Junkasem, R. Rujiravanit, P. Supaphol, Fabrication of α-chitin whisker-reinforced poly(vinyl alcohol) nanocomposite nanofibres by electrospinning, Nanotechnology. 17 (2006) 4519–4528. https://doi.org/10.1088/0957-4484/17/17/039.

[9] S. Azizi, M. Bin Ahmad, N. A. Ibrahim, M. Z. Hussein, F. Namvar, Preparation and properties of poly(vinyl alcohol)/chitosan blend bio-

nanocomposites reinforced by cellulose nanocrystals, Chinese J. Polym. Sci. 32 (2014) 1620–1627. https://doi.org/10.1007/s10118-014-1548-0.

[10] M. I. Baker, S. P. Walsh, Z. Schwartz, B. D. Boyan, A review of polyvinyl alcohol and its uses in cartilage and orthopedic applications, J. Biomed. Mater. Res. Part B Appl. Biomater. 100B (2012) 1451–1457. https://doi.org/10.1002/jbm.b.32694.

[11] M. S. Peresin, Y. Habibi, J. O. Zoppe, J. J. Pawlak, O. J. Rojas, Nanofiber Composites of Polyvinyl Alcohol and Cellulose Nanocrystals: Manufacture and Characterization, Biomacromol. 11 (2010) 674–681. https://doi.org/10.1021/bm901254n.

[12] G. Hirankumar, S. Selvasekarapandian, N. Kuwata, J. Kawamura, T. Hattori, Thermal, electrical and optical studies on the poly(vinyl alcohol) based polymer electrolytes, J. Power Sources. 144 (2005) 262–267. https://doi.org/10.1016/j.jpowsour.2004.12.019.

[13] A. L. Saroj, S. Krishnamoorthi, R. K. Singh, Structural, thermal and electrical transport behaviour of polymer electrolytes based on PVA and imidazolium based ionic liquid, J. Non. Cryst. Solids. 473 (2017) 87–95. https://doi.org/10.1016/j.jnoncrysol.2017.07.035.

[14] S. Kumar, G. K. Prajapati, A. L. Saroj, P. N. Gupta, Structural, electrical and dielectric studies of nano-composite polymer blend electrolyte films based on $_{(70-x)}$PVA–$_{x}$PVP–NaI–SiO_2, Phys. B Condens. Matter. 554 (2019) 158–164. https://doi.org/10.1016/j.physb.2018.11.010.

[15] T. Dippel, K. Kreuer, J. Lassegues, D. Rodriguez, Proton conductivity in fused phosphoric acid; A1H/31P PFG-NMR and QNS study, Solid State Ionics. 61 (1993) 41–46. https://doi.org/10.1016/0167-2738(93)90332-W.

[16] S. Celik, A. Aslan, A. Bozkurt, Phosphoric acid-doped poly(1-vinyl-1,2,4-triazole) as water-free proton conducting polymer electrolytes, Solid State Ionics. 179 (2008) 683–688. https://doi.org/10.1016/j.ssi.2008.04.033.

[17] F. Ahmad, E. Sheha, Preparation and physical properties of $(PVA)_{0.7}(NaBr)_{0.3}(H_3PO_4)_{xM}$ solid acid membrane for phosphoric acid - Fuel cells, J. Adv. Res. 4 (2013) 155–161. https://doi.org/10.1016/j.jare.2012.05.001.

[18] B. Scrosati, F. Croce, L. Persi, Impedance Spectroscopy Study of PEO-Based Nanocomposite Polymer Electrolytes, J. Electrochem. Soc. 147

(2000) 1718. https://doi.org/10.1149/1.1393423.

[19] S. H. Chung, Y. Wang, L. Persi, F. Croce, S. G. Greenbaum, B. Scrosati, E. Plichta, Enhancement of ion transport in polymer electrolytes by addition of nanoscale inorganic oxides, J. Power Sources. 97–98 (2001) 644–648. https://doi.org/10.1016/S0378-7753(01)00748-0.

[20] C. Z. Wang, K. M. Ho, Structure, dynamics, and electronic properties of diamondlike amorphous carbon, Phys. Rev. Lett. 71 (1993) 1184–1187. https://doi.org/10.1103/PhysRevLett.71.1184.

[21] L. Calcagno, G. Foti, Density enhancement in ion implanted polymers, Nucl. Instruments Methods Phys. Res. Sect. B Beam Interact. with Mater. Atoms. 19–20 (1987) 895–898. https://doi.org/10.1016/S0168-583X(87)80179-9.

[22] Y. J. Park, Y. S. Kang, C. Park, Micropatterning of semicrystalline poly(vinylidene fluoride) (PVDF) solutions, Eur. Polym. J. 41 (2005) 1002–1012. https://doi.org/10.1016/j.eurpolymj.2004.11.022.

[23] A. A. El-Saftawy, A. M. Abdel Reheem, S. A. Kandil, S. A. Abd El Aal, S. Salama, Comparative studies on PADC polymeric detector treated by gamma radiation and Ar ion beam, Appl. Surf. Sci. 371 (2016) 596–606. https://doi.org/10.1016/j.apsusc.2016.03.044.

[24] S. Bhavsar, G. B. Patel, N. L. Singh, B. Singh, F. Singh, Effect of Gamma and 90 MeV Carbon ions on Optical properties of PVA/H_3PO_4/SiO_2 Nanocomposite Polymer Electrolytes. (To be Communicate)

[25] S. Bhavsar, G. B. Patel, N. L. Singh, B. Singh, F. Singh, Influence of Gamma and 90 MeV Carbon ions on Structural, Thermal and Electrical properties of PVA/H_3PO_4/SiO_2 Nanocomposite Polymer Electrolytes. (To be Communicate)

[26] A. G. El-Shamy, Composite (PVA/Cu nano) films: Two yield points, embedding mechanism and thermal properties, Prog. Org. Coatings. 127 (2019) 252–259. https://doi.org/10.1016/j.porgcoat.2018.11.024.

[27] R. K. Dhillon, P. Singh, S. K. Gupta, S. Singh, R. Kumar, Study of high energy (MeV) N^{6+} ion and gamma radiation induced modifications in low density polyethylene (LDPE) polymer, Nucl. Instruments Methods Phys. Res. Sect. B Beam Interact. with Mater. Atoms. 301 (2013) 12–16. https://doi.org/10.1016/j.nimb.2013.02.014.

[28] G. B. Patel, N. L. Singh, F. Singh, P. K. Kulriya, Effects of MeV ions on physicochemical and dielectric properties of chitosan / PEO polymeric blend, Nucl. Inst. Methods Phys. Res. B. 447 (2019) 68–78. https://doi.org/10.1016/j.nimb.2019.03.052.

[29] K. N. Kumar, R. Padma, Y. C. Ratnakaram, M. Kang, Bright green emission from f-MWCNT embedded co-doped Bi^{3+} + Tb^{3+} :polyvinyl alcohol polymer nanocomposites for photonic applications, RSC Adv. 7 (2017) 15084–15095. https://doi.org/10.1039/C7RA01007A.

[30] J. Jiang, D. Gao, Z. Li, G. Su, Gel polymer electrolytes prepared by in situ polymerization of vinyl monomers in room-temperature ionic liquids, React. Funct. Polym. 66 (2006) 1141–1148. https://doi.org/10.1016/j.reactfunctpolym.2006.02.004.

[31] W. Bolse, Self-organised nano-structuring of thin oxide-films under swift heavy ion bombardment, Nucl. Instruments Methods Phys. Res. Sect. B Beam Interact. with Mater. Atoms. 244 (2006) 8–14. https://doi.org/10.1016/j.nimb.2005.11.007.

[32] R. P. Chahal, S. Mahendia, A. K. Tomar, S. Kumar, γ-Irradiated PVA/Ag nanocomposite films: Materials for optical applications, J. Alloys Compd. 538 (2012) 212–219. https://doi.org/10.1016/j.jallcom.2012.05.085.

[33] J. Tauc, R. Grigorovici, A. Vancu, Optical Properties and Electronic Structure of Amorphous Germanium, Phys. Status Solidi. 15 (1966) 627–637. https://doi.org/10.1002/pssb.19660150224.

[34] N. F. Mott, E. A. Davis, Electronic Processes in Non Crystalline Materials, Clarendon Press, Oxford, 1979.

[35] D. Fink, W. H. Chung, R. Klett, A. Schmoldt, J. Cardoso, R. Montiel, M. H. Vazquez, L. Wang, F. Hosoi, H. Omichi, P. Goppelt-Langer, Carbonaceous clusters in irradiated polymers as revealed by UV-Vis spectrometry, Radiat. Eff. Defects Solids. 133 (1995) 193–208. https://doi.org/10.1080/10420159508223990.

[36] M. F. Shukur, R. Ithnin, H. A. Illias, M. F. Z. Kadir, Proton conducting polymer electrolyte based on plasticized chitosan – PEO blend and application in electrochemical devices, Opt. Mater. 35 (2013) 1834–1841. https://doi.org/10.1016/j.optmat.2013.03.004.

[37] A. Arya, A. L. Sharma, Structural, electrical properties and dielectric

relaxations in Na^+ -ion-conducting solid polymer electrolyte, J. Phys. Condens. Matter. 30 (2018) 165402. https://doi.org/10.1088/1361-648X/aab466.

[38] E. Lee, G. Rao, L. Mansur, LET effect on cross-linking and scission mechanisms of PMMA during irradiation, Radiat. Phys. Chem. 55 (1999) 293–305. https://doi.org/10.1016/S0969-806X(99)00184-X.

[39] N. L. Singh, A. Sharma, D. K. Avasthi, V. Shrinet, Temperature and frequency dependent electrical properties of 50 MeV Li^{3+} ion irradiated polymeric blends, Radiat. Eff. Defects Solids. 160 (2005) 99–107. https://doi.org/10.1080/10420150500116649.

[40] N. A. Peppas, E. W. Merrill, Differential scanning calorimetry of crystallized PVA hydrogels, J. Appl. Polym. Sci. 20 (1976) 1457–1465. https://doi.org/10.1002/app.1976.070200604.

[41] G. B. Patel, S. Bhavsar, N. L. Singh, F. Singh, P. K. Kulriya, SHI induced modification in structural, optical, dielectric and thermal properties of poly ethylene oxide films, Nucl. Instruments Methods Phys. Res. Sect. B Beam Interact. with Mater. Atoms. 379 (2016) 156–161. https://doi.org/10.1016/j.nimb.2016.04.018.